HSurf-Net: Normal Estimation for 3D Point Clouds by Learning Hyper Surfaces

Anonymous Author(s)
Affiliation
Address
email

Abstract

We propose a novel normal estimation method called HSurf-Net, which can accurately predict normals from point clouds with noise and density variations. Previous methods focus on learning point weights to fit neighborhoods into a geometric surface approximated by a polynomial function of a predefined order, based on which normals are estimated. However, fitting surfaces explicitly from raw point clouds suffers from overfitting or underfitting issues caused by inappropriate polynomial orders and outliers, which significantly limits the performance of the existing methods. To address these issues, we introduce hyper surface fitting to implicitly learn *hyper surfaces*, which are represented by multi-layer perceptron (MLP) layers that take point features and output surface patterns in a high dimensional feature space. We employ a novel space transformation module, which consists of a sequence of local aggregation layers and global shift layers, to reliably build the feature space, and a relative position encoding module to effectively convert the point clouds into that feature space. Our model learns hyper surfaces from the noise-less features and directly predicts normal vectors. We jointly optimize the MLP weights and module parameters in a data-driven manner to make the model adaptively find the most suitable surface pattern for various points. Experimental results show that our HSurf-Net achieves state-of-the-art (SOTA) performance on the synthetic shape dataset, the real-world indoor and outdoor scene datasets.

1 Introduction

Estimating normals from point clouds is vital for various downstream applications of 3D computer vision, such as point cloud filtering [5, 42, 32, 31], surface reconstruction [25] and rendering/shading [8, 14, 36]. Though this topic has been extensively studied, it is still a challenge to work on point clouds with different types of noise, outliers, and density variations. It is well-known that point cloud normal estimation can be formulated as the least squares optimization problem, which explicitly fits a geometric surface (e.g. plane and polynomial surface) on local neighboring points and then computes the normal from the fitted surface. Specifically, the point-wise weights dedicate the importance of each point for the surface fitting.

Existing normal estimation algorithms can be roughly divided into two categories: traditional methods and learning-based methods. The traditional ones usually approximate potential structural properties of point clouds and use a well-designed algorithm to fit local planes or polynomial surfaces [20, 12]. However, explicitly fitting geometric surfaces heavily rely on careful parameters tuning, such as the neighborhood size and the order of polynomial function. The learning-based ones initially try

Submitted to 36th Conference on Neural Information Processing Systems (NeurIPS 2022). Do not distribute.

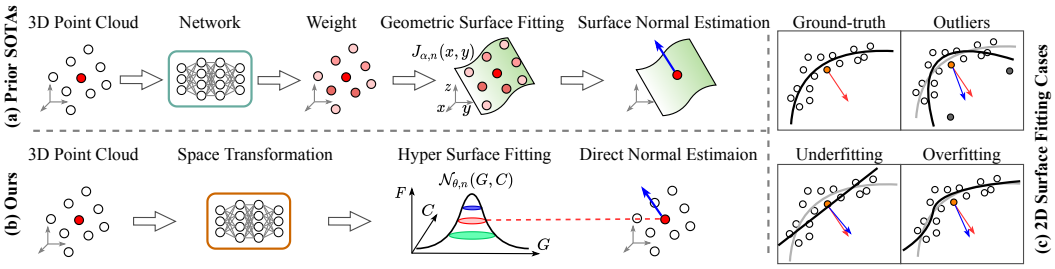

Figure 1: (a) Prior SOTA methods focus on weight learning and geometric surface fitting to estimate the surface normal. (b) We use features G, C to learn a hyper surface $\mathcal{N}_{\theta,\tau}(G, C)$ to directly estimate normal for each point. (c) Existing surface fitting techniques are severely affected by overfitting, underfitting and outliers, which lead to inaccurate surface approximation and normal estimation.

to directly predict normal vectors from point clouds through regression network [10, 16, 7, 48, 47]. Alternatively, recent methods employ Convolutional Neural Networks (CNN) [28] or the PointNet architecture [6, 50] to learn point-wise weights, then the classic geometric surface fitting is utilized to compute normals (see Fig. 1(a)). The learning-based regression methods lack geometric prior and are hard to learn a general mapping from severely degraded inputs to the ground-truth normals, especially for complex geometric structures. For the learning-based surface fitting methods, one issue of these approaches is that explicit surface fitting is sensitive to noise and outliers. The weights on noisy points that are far away from the underlying surface than inlier points significantly affect the accuracy of normals, even small weights on outliers still will result in an erroneous normal estimation. Another inherent issue is that their predefined polynomial functions may lead to inconsistency between the various underlying surfaces and their fitted surfaces, where a constant order is selected for all points, e.g. plane in [28, 11] and 3-jet surface in [6, 50]. If the selected order is smaller than the order of the underlying surface, it will result in an underfitting, which smooths out the fine details and affects the accuracy of output normals. Otherwise, overfitting makes the algorithm sensitive to noise and brings instability to the normal estimation [50]. The 2D example is illustrated in Fig. 1(c).

To address these issues, we propose a new unoriented normal estimation network called *HSurf-Net*. It makes full use of the powerful learning ability of the neural network to implicitly learn hyper surfaces, which are represented by MLP layers and the learnable parameters of the layers interpret the geometric structures in a high dimensional feature space. The advantage is that the hyper surfaces can adaptively fit more complex point patterns in a robust way. Based on the hyper surfaces, we introduce a *Hyper Surface Fitting* module to directly predict normal vectors (see Fig. 1(b)). This module learns from the well extracted point features and optimizes the surface representation parameters in a data-driven manner, rather than explicitly fitting 3D planes/surfaces approximated by a polynomial function of a predefined order. Moreover, to avoid the selection of neighborhood scale and construct a noise-less feature space, we design two network modules called *Space Transformation* and *Relative Position Encoding*. They benefit from local, small and large scales to enhance the extraction of structure-aware and multi-scale features. Overall, the combination of these modules well extracts the geometric information and avoids the issues caused by explicit polynomial surface fitting, thus improving the effectiveness of the normal estimation framework. We conduct evaluation experiments on the synthetic shape dataset, the real-world indoor and outdoor scene datasets. HSurf-Net significantly outperforms other baselines on the challenging cases in these benchmarks. Extensive ablation experiments also validate the effect of each component that contributes to the final results.

Our main contributions can be summarized as follows.

- A technique for representing polynomial surfaces of a predefined order based on 3D space as hyper surfaces, which are parameterized as MLP layers.
- A Hyper Surface Fitting in a high dimensional feature space to optimize this surface representation for point cloud normal estimation, which brings more robustness and accuracy to the estimation.
- A Space Transformation module and a Relative Position Encoding module to map 3D point clouds into the feature space. They are combined to fully explore the local geometry and extract features from different neighborhood scales.

2 Related Work

Traditional Normal Estimation. The classic point cloud normal estimation methods use plane fitting techniques, such as unweighted Principle Component Analysis (PCA) [20] and Singular Value Decomposition (SVD) [41]. They analyze the covariance matrix in a local patch around a point and define its normal as the eigenvector corresponding to the smallest eigenvalue. Subsequently, a variety of PCA-variants [1, 35, 34, 26, 22] have been proposed to improve the accuracy. In order to preserve sharp features and retain more details, a lot of improvements extract normals by using Voronoi cells [3, 33], Voronoi-PCA [13, 2], Hough transform [9] and edge-aware sampling [23]. In addition, some methods utilize more complex surface reconstruction techniques, such as Moving Least Squares (MLS) [29], jet fitting [12], local spherical fitting [15] and multi-scale kernel [4]. The aforementioned approaches come with certain assumptions or specific observations, and hold theoretical guarantees on approximation and robustness. Besides, these approaches need a fine-tuned set of parameters according to the input point clouds.

Learning-based Normal Estimation. (1) *Regression based methods*. Initially, some learning-based methods propose to directly regress normal vectors from raw point clouds. HoughCNN [10] transforms the 3D points into a 2D grid representation via Hough transform, and then use a CNN to select a normal direction from the accumulator in Hough space. Similarly, Roveri *et al*. [39] define a grid-like regular input to learn point normals. Lu *et al*. [30] project each point into a 2D height map by computing the distances between points and the PCA fitted plane. Above investigated methods map the unstructured point cloud data into a regular domain, which may lose or alter the 3D geometric information. Instead, the following approaches learn from raw point clouds. PCPNet [16] applies the PointNet architecture [37] in a local patch-based multi-scale form to estimate normals and curvatures from point clouds. Hashimoto *et al*. [19] propose a two-branch network that extracts local and spatial features, which are integrated to learn normals. Nesti-Net [7] proposes to parameterize the local field as a multi-scale feature vector, then uses a mixture-of-experts architecture [24] to find the optimal neighborhood scale around each point, but it is very time consuming. Based on PCPNet, Zhou *et al*. [48] introduce an extra plane feature constraint and a multi-scale neighborhood selection strategy to improve the performance. Refine-Net [46, 47] first computes an initial normal at each point by searching a ideal fitting patch. Then, a refinement network is used to obtain the final optimal normals by incorporating the learned local point features and the constructed height map features. (2) *Surface fitting based methods*. Recent normal estimation methods try to combine traditional plane/surface fitting techniques with learning-based methods. Lenssen *et al*. [28] propose a fast algorithm that utilizes an adaptive anisotropic kernel to iteratively refine a weighted least squares plane fitting. MTRNet [11] proposes a differentiable RANSAC-like module to predict a latent tangent plane. DeepFit [6] and AdaFit [50] both employ a Taylor expansion to describe the local surface and use the PointNet to predict point-wise weights for a weighted least squares surface fitting. In addition, AdaFit proposes to use a novel layer to aggregate features from multiple neighborhood sizes and add offset to point coordinates to further improve the results. Similarly, Zhou *et al*. [49] use the learned weights and features to select local top-k points and update the point positions. Zhang *et al*. [44] introduce geometric weight guidance to provide more reliable inlier points for plane fitting.

Compared to the learning-based normal regression methods, e.g. PCPNet, Nesti-Net and Refine-Net, which focus on learning a general mapping from the inputs to the ground-truth normals, our approach is greatly improved by deploying a hyper surface fitting to explore geometric prior supports in high dimensional space. Compared to the learning-based surface fitting methods, e.g. DeepFit and AdaFit, which solve a 3D space based polynomial function of a predefined order to get normals, we effectively improve the results by learning hyper surfaces in a feature space.

3 Method

Given a local point set $P = \{p_i | i = 1, ..., N\}$ centralized at a query point p, our algorithm aims to estimate the unoriented normal $\mathbf{n}_p$ at point p. Fig. 2 shows an overview of the proposed approach. First, to remove unnecessary degrees of freedom from the input data space and lower the learning

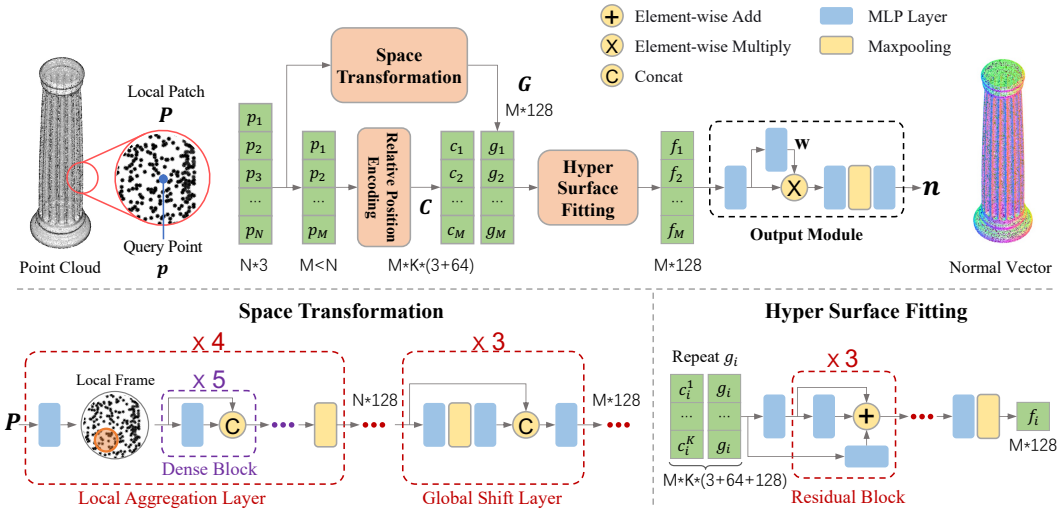

Figure 2: The architecture of HSurf-Net for point cloud normal estimation.

difficulty, we normalize each point coordinate with its patch radius and rotate the points into a local coordinate system defined by the PCA. Then, the Space Transformation module extracts a *global location code* G for each point (Sec. 3.3). Moreover, local frames are formulated at point p_i based on spatial coordinates and are used to compute a *condition code* C by a Relative Position Encoding module (Sec. 3.4). After that, we perform the hyper surface fitting in a high dimensional feature space (Sec. 3.2). Finally, we recover the 3D normal vectors from fitting results by an Output Module.

3.1 Preliminary

We first briefly review the formulas and mathematical notations of the explicit surface fitting with a polynomial function of a predefined order. A smooth surface can be locally formulated as the graph of a bivariate height function $f(x, y)$ about the z-axis that is not in the *tangent space* [40, 27]. An n-order Taylor expansion of the height function over a surface is given by

$$f(x,y) = J_{\beta,n}(x,y) + O(||(x,y)||^{n+1}), \quad \text{where } J_{\beta,n}(x,y) = \sum_{k=0}^{n}\sum_{j=0}^{k} \beta_{k-j,j} x^{k-j} y^{j}. \tag{1}$$

The polynomial function $J_{\beta,n} : \mathbb{R}^2 \rightarrow \mathbb{R}$ is the truncated Taylor expansion called n-jet [12]. β is the n-jet coefficient vector and involves $N_n = (n+1)(n+2)/2$ terms. $O(\cdot)$ denotes the remainder in Taylor's multivariate formula. The predefined order n determines the complexity of the fitted surface.

Given a collection of points $P = \{p_i = (x_i, y_i, z_i) | i = 1, ..., N\}$ around its origin p on a sampled smooth surface S. Consider the height function $z = f(x, y)$ given by Eq. (1) in the defined coordinate system. The n-order differential property of the surface $S = f(x_i, y_i)$ at point p_i can be investigated by interpolating S using a bivariate n-jet $J_{\alpha,n}(x, y)$, such that

$$f(x_i, y_i) \simeq J_{\alpha,n}(x_i, y_i), \quad \forall i = 1, ..., N\ , \tag{2}$$

where α means the coefficient of the jet sought. Thus, the coefficient α is the solution of the n-jet surface fitting and is denoted as N_n-vector $\alpha = (\alpha_{0,0}, \alpha_{1,0}, \alpha_{0,1}, ..., \alpha_{0,n})^T$. To find the solution, the least squares approximation strategy is used to minimize the sum of the square errors between the jet value and the height function over the point set P

$$J^*_{\alpha,n} = \underset{\alpha}{\operatorname{argmin}} \sum_{i=1}^{N} (f(x_i, y_i) - J_{\alpha,n}(x_i, y_i))^2. \tag{3}$$

Then the surface fitting problem of Eq. (2) is described as finding the least squares solution of a homogeneous system of linear equations. Once the n-jet coefficient α is solved, the normal vector at point p on the fitted surface is computed by

$$\mathbf{n}_p = h(\alpha) = (-\alpha_{1,0}, -\alpha_{0,1}, 1)/\sqrt{1 + \alpha_{1,0}^2 + \alpha_{0,1}^2}\ . \tag{4}$$

3.2 Hyper Surface Fitting

The explicit surface fitting method in Sec. 3.1 requires a predefined polynomial function of an order n and its performance is susceptible to noise and outliers, as shown in Sec. 4.3. Motivated by the rapidly developed data-driven approaches, which excel at adaptively learning a fitting model that describes the pattern of the provided noisy data, we propose to implicitly learn hyper surfaces in the *feature space* using a *Hyper Surface Fitting* technique. We expand the 3D point coordinates (x, y, z) into high dimensional features (G, C, F), and $F \sim \mathcal{F}(G, C), F \in \mathbb{R}^c$. Then the new feature-based formulation for the polynomial function $J_{\alpha,n}(x, y)$ in Eq. (2) is given by

$$\begin{aligned} \mathcal{N}_{\theta,\tau}(G, C) &= \sum_{k=0}^{\tau} \sum_{j=0}^{k} \theta_{k-j,j}\, G^{k-j} C^{j} \\ &= \theta_{0,0} + \theta_{1,0} G + \theta_{0,1} C + ... + \theta_{1,\tau-1} G C^{\tau-1} + \theta_{0,\tau} C^{\tau} \ , \end{aligned} \tag{5}$$

where $G \in \mathbb{R}^c$ and $C \in \mathbb{R}^c$ are features of the 3D point clouds along two different basis vectors in the feature space, which are introduced in the following sections. Here, the order τ and the coefficient θ are parameters of an MLP-based module, which is designed as a sequence of skip-connected Residual Block units (see Fig. 2). Similar with Eq. (3), the bivariate function $\mathcal{N}_{\theta,\tau}(G, C)$ aims to map each feature pair (G_i, C_i) to their "true height" $\mathcal{F}(G_i, C_i) \in \mathbb{R}^c$ in the feature space

$$\mathcal{N}^*_{\theta,\tau} = \underset{\theta,\tau}{\operatorname{argmin}} \sum_{i=1}^{N} \|\mathcal{N}_{\theta,\tau}(G_i, C_i) - \mathcal{F}(G_i, C_i)\|^2. \tag{6}$$

In contrast to compute point normals formulaically by the n-jet coefficients as in Eq. (4), we recover the normal vectors $\mathbf{n}$ from the c-dimensional hyper surface using a function $\mathcal{H} : \mathbb{R}^c \rightarrow \mathbb{R}^3$, which is applied to the fitting surface and the surface of fitting sought, i.e. the ground-truth surface

$$\mathcal{N}^*_{\theta,\tau} = \underset{\theta,\tau}{\operatorname{argmin}} \sum_{i=1}^{N} \|\mathcal{H}(\mathcal{N}_{\theta,\tau}(G_i, C_i)) - \mathcal{H}(\mathcal{F}(G_i, C_i))\|^2. \tag{7}$$

Then we get the optimization function about the normals

$$\mathcal{N}^*_{\theta,\tau} = \underset{\theta,\tau}{\operatorname{argmin}} \sum_{i=1}^{N} \|\mathbf{n}_i - \hat{\mathbf{n}}_i\|^2, \tag{8}$$

where $\mathbf{n}$ and $\hat{\mathbf{n}}$ are the output unoriented normal and the ground-truth, respectively. Finally, the normal of the query point p is formulated as the weighted maxpooling of its neighborhoods (see *Output Module* in Fig. 2)

$$\mathbf{n}_p = \|\mathcal{H}(\mathrm{MAX}\{w_i\, \mathcal{N}_{\theta,\tau}(G_i, C_i) | i = 1, ..., N\})\|, \tag{9}$$

where $\mathrm{MAX}\{\cdot\}$ means maxpooling, $w_i = \mathrm{sigmod}(\Psi(\mathcal{N}_{\theta,\tau}(G_i, C_i)))$ is weight, $\mathcal{H}$ and Ψ are MLPs. We experimentally find that sin distance $|\hat{\mathbf{n}}_p \times \mathbf{n}_p|$ is more suitable for measuring the vector difference and guiding the estimated normal to match the ground-truth (see Sec. 4.3). Our method adaptively learns the optimal hyper surface $\mathcal{N}^*_{\theta,\tau}$ from high dimensional features, and it is more robust than the n-jet fitting, which fits a single type of surface from 3D points with a constant order.

3.3 Space Transformation

The previous methods usually use the PointNet-like architectures to learn features from point clouds. Since PointNet is inadequate for encoding local structures, we design a feature extraction module called *Space Transformation*, which learns from local neighborhood, small and large patch scales. This module provides a noise-less *global location code* G for the hyper surface fitting, and it consists of a sequence of Local Aggregation Layer units and Global Shift Layer units (see Fig. 2). We repeatedly employ each kind of unit on different levels of feature representation details. The raw point clouds are often noisy and the points have position offsets relative to the noise-free points, which will lead to deviation in the learned features. The Local Aggregation Layer delivers a smooth filtered

relative feature of each point by the cascaded local frame construction and maxpooling operation. Since the relative features only describe the local structures, we design a Global Shift Layer to provide the final features with global position information in the feature space by fusing global features. Specifically, we explore the global information from different scales, as shown in Fig. 3.

In the *Local Aggregation Layer*, we first convert the input points to a fixed dimension. Then, we group the local neighborhood features at each point by the 3D spatial distance based kNN search, and refine each grouped feature via a chain of Dense Block units. Finally, we compute an order-invariant per-point feature via maxpooling operation [38]. In the Dense Block, we use the skip-connection to leverage features extracted across different layers. In this way, the information of different layers is combined via intra-level connections inside the unit, which realizes the information reuse, thereby improving the description ability of the network.

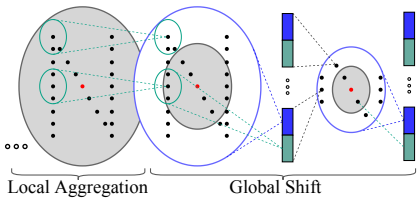

Figure 3: Space Transformation module.

In the *Global Shift Layer*, we provide the localization of points in the entire patch feature space by fusing global features extracted from multiple neighborhood size scales of the query point p. Extracting multi-scale features has become an effective strategy to further boost the normal estimation performance [10, 7, 16, 48, 11, 50]. The small scale results in a more accurate description of the details, while the large scale provides more information about the underlying geometries. In summary, our scale-aware Global Shift Layer is formulated as (see the blue part in Fig. 3)

$$G_{s+1,i} = \mathcal{U}_s(\mathcal{V}_s(\mathrm{MAX}\{G_{s,j}|j=1,..,N_s\}),\ G_{s,i}),\ i=1,...,N_{s+1}\ , \tag{10}$$

where $\mathcal{U}, \mathcal{V}$ are MLP layers, $G_{s,i}$ is the per-point feature at scale s. $\mathrm{MAX}\{\cdot\}$ means performing feature maxpooling over all neighboring points of p with size N_s and $N_{s+1} \leq N_s$.

3.4 Relative Position Encoding

Position encoding is important for the transformer architecture [43, 17, 45], allowing the self-attention mechanism to capture sequence order information of input tokens. We borrow the idea and use it here to extract a *condition code* C from the local geometry of point cloud data. Contrast to the traditional position encoding, which manually craft for language sequence or image grid based on sine and cosine functions, we design a parameterized and learnable encoding scheme which is trained together with the whole model. Given a point $p_i \in \{p_i|i=1,...,M\}$ and its neighborhoods $\{p_i^j|j=1,...,N_k\}$, our learning-based position encoding function ϕ using relative coordinates is formulated as

$$C_i^j = \phi(p_i^j - p_i,\ \mathcal{E}(p_i^j - p_i)), \tag{11}$$

where $p_i^j - p_i$ denotes the relative position in a local frame, and $M = N/4$ neighboring points of p is selected. The encoding functions $\mathcal{E}$ and ϕ are MLP layers. Experimental results show that our encoding scheme outperforms the traditional position encoding in the normal estimation task.

4 Experiments

Datasets and Settings. We first compare our method with other baselines using same train/test data of PCPNet shape dataset [16]. To evaluate the generalization ability of each method on the real-world scene data, we employ the models pretrained on the PCPNet dataset to report results on the indoor SceneNN dataset [21] and the outdoor Semantic3D dataset [18]. For PCPNet dataset, we follow the experimental setup in [16] including train/test set split, data noise, density variations and augmentation. We randomly sample 1000 query points for each shape during training. We set the initial point cloud patch size $N = 700$ and scale set $N_s = \{N, N/2, N/4\}$. The number of kNN points in the Space Transformation is 16 and in the encoding module $N_k = 16$. We use Adam optimizer with initial learning rate 5×10^{-4} and the learning rate is decayed to 0.2 of the latest value after every 200 epochs. The model is trained with a batch size of 100 in 900 epochs on a Nvidia 2080 Ti GPU. More information about the datasets and evaluation metrics can be found in the supplementary materials.

Table 1: Normal angle RMSE results on the PCPNet and SceneNN dataset. Sorted by the average values on the PCPNet dataset. Lower is better. $*$ means the code is not available or uncompleted.

Category	PCPNet Dataset							SceneNN Dataset		
	Noise σ				Density		**Average**	Clean	Noise	**Average**
	None	0.12%	0.6%	1.2%	Stripes	Gradient				
Jet [12]	12.35	12.84	18.33	27.68	13.39	13.13	16.29	15.17	15.59	15.38
PCA [20]	12.29	12.87	18.38	27.52	13.66	12.81	16.25	15.93	16.32	16.12
PCPNet [16]	9.64	11.51	18.27	22.84	11.73	13.46	14.58	20.86	21.40	21.13
Zhou *et al.** [48]	8.67	10.49	17.62	24.14	10.29	10.66	13.62	-	-	-
Nesti-Net [7]	7.06	10.24	17.77	22.31	8.64	8.95	12.49	13.01	15.19	14.10
Lenssen *et al.* [28]	6.72	9.95	17.18	21.96	7.73	7.51	11.84	10.24	13.00	11.62
DeepFit [6]	6.51	9.21	16.73	23.12	7.92	7.31	11.80	10.33	13.07	11.70
MTRNet* [11]	6.43	9.69	17.08	22.23	8.39	6.89	11.78	-	-	-
Refine-Net [47]	5.92	9.04	16.52	22.19	7.70	7.20	11.43	18.09	19.73	18.91
Zhang *et al.** [44]	5.65	9.19	16.78	22.93	6.68	6.29	11.25	9.31	13.11	11.21
Zhou *et al.** [49]	5.90	9.10	16.50	22.08	6.79	6.40	11.13	-	-	-
AdaFit [50]	5.19	9.05	16.45	21.94	6.01	5.90	10.76	8.39	12.85	10.62
Ours	**4.17**	**8.78**	**16.25**	**21.61**	**4.98**	**4.86**	**10.11**	**7.55**	**12.23**	**9.89**

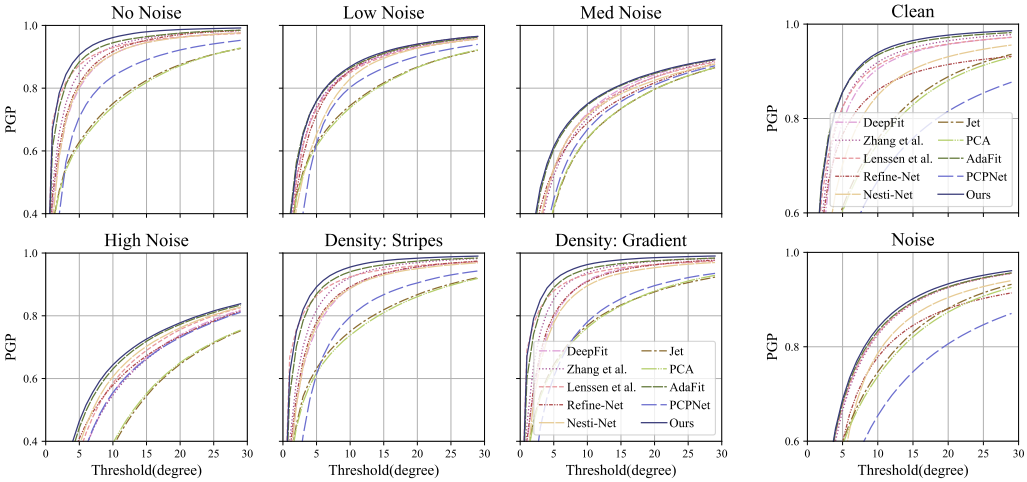

(a) PCPNet Dataset (b) SceneNN Dataset

Figure 4: Normal error AUC results on the PCPNet and SceneNN dataset. X-axis is the angle threshold in degree and Y-axis is the percentage of good point (PGP) normals under a given threshold.

4.1 Results on Synthetic Shape Dataset

Table 1 reports numerical comparison in terms of Root Mean Squared Error (RMSE) on the PCPNet dataset [16]. Fig. 4(a) shows the normal error Area Under the Curve (AUC) results. It can be seen that our method consistently outperforms both the traditional methods and learning-based methods across all noise levels and density variations. The results also show that the performance of all methods degrade substantially as the noise level increases, but the influence of density variations is much smaller than the noise. Fig. 5(a) shows the visual comparison on different shapes, where the point clouds are rendered with a normal angle error map. We can see that errors mostly occur in regions with complex geometry or high curvature, e.g. edges and corners. Our method shows smallest errors on these regions due to its hyper surface fitting in a high dimensional feature space, enabling it to adapt to the different local geometry and disregard irrelevant outliers. In the supplemental materials, we provide more evaluation results and subsequent applications of normal estimation.

4.2 Results on Indoor and Outdoor Scene Datasets

Table 1 presents numerical comparison with the state-of-the-art results in terms of RMSE on the SceneNN dataset [21]. Fig. 4(b) shows the normal angle error AUC results. Fig. 5(b) visualizes the

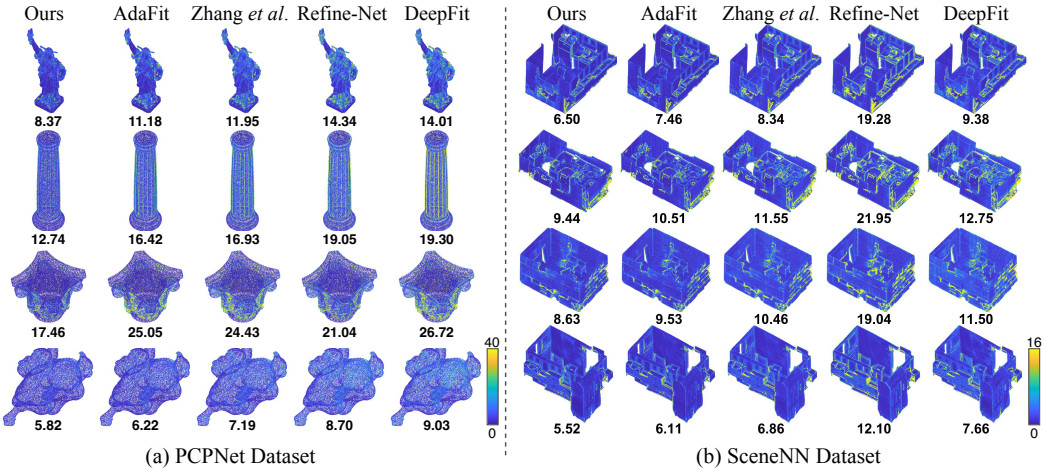

Figure 5: Error visualization results on the PCPNet complex shapes and SceneNN dataset. The number under each point cloud is its RMSE. The point color is the angular error mapped to a heatmap.

qualitative comparison of errors in different room scenes. The quantitative and qualitative comparison results show that our method outperforms both the traditional and the learning-based methods in all scenes and data categories.

In Fig. 6, we show visual comparison on the Semantic3D dataset [18] as the absence of the ground-truth normal. We can observe that our method preserve fine details in the complex structures of the building, such as sharp edge, groove between the bricks, pattern and relief on the wall, while other methods behave over-smooth in these areas or give wrong normals. The comparison results demonstrate that our method can be well generalized to the real-world LiDAR data.

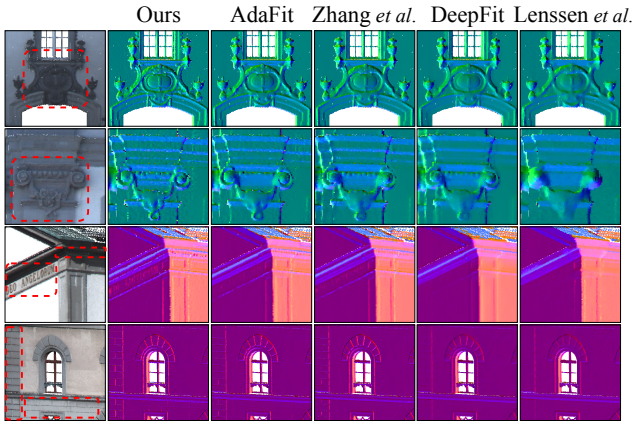

Figure 6: Visual comparison on the Semantic3D dataset. The point normal vectors are mapped to RGB colors.

4.3 Ablation Study

(a) Hyper Surface Fitting. To validate the effectiveness of the proposed hyper surface fitting technique, we compare the performance of different models with the n-jet fitting and our hyper surface fitting. The same backbone network (i.e. space transformation and position encoding) is used in this experiment, but the inputs of the jet fitting based models are 3D points and point-wise weights, which are predicted by the backbone network. We also evaluate a model that replaces the residual block in our hyper surface fitting module with a concat operation, and we call it “Simple". The results are shown in Table 2(a), we can see that the performance of the models with jet fitting is sensitive to the polynomial order n, while the hyper surface fitting can effectively improve the performance. Moreover, a simple 1-order may be enough for the n-jet fitting in the normal estimation task.

(b) Space Transformation. Our Space Transformation is composed of connected Local Aggregation Layer units and Global Shift Layer units. In Table 2(b), we conduct feature extraction experiments using two types of the Space Transformation: 1) with a PointNet based aggregation layer; 2) without the multi-scale Global Shift Layer and with a fixed scale N'. The results show that the newly designed components can effectively boost the normal estimation performance.

(c) Encoding Module. In Table 2(c), we provide the results with the traditional position encoding in [43]. We also provide the results of a model that directly uses the 3D point coordinates as the

Table 2: Normal angle RMSE results of ablation studies on the PCPNet dataset. The ablation experiments include: our new designed modules, i.e. (a) Hyper Surface Fitting, (b) Space Transformation, (c) Relative Position Encoding and (d) Output Module, and a hyperparameter, i.e. (e) the input point cloud patch size. Please see the text for more details.

Ablation		Hyper Surface	Space Trans.	Position Encoding	Output Module	**Noise σ** None	0.12%	0.6%	1.2%	**Density** Stripes	Gradient	**Average**
(a)	Jet $n=1$		✓	✓	✓	7.55	9.95	16.54	21.99	8.89	7.83	12.12
	Jet $n=2$		✓	✓	✓	8.52	10.13	16.59	22.12	10.09	9.05	12.75
	Jet $n=3$		✓	✓	✓	7.50	9.70	16.68	22.22	9.01	8.07	12.19
	Simple		✓	✓	✓	4.44	8.84	16.29	21.76	5.27	5.18	10.30
(b)	PointNet-based	✓		✓	✓	4.84	9.09	16.47	21.98	5.67	5.63	10.61
	$N'=256$	✓		✓	✓	5.56	9.19	16.76	23.20	6.71	6.21	11.27
	$N'=500$	✓		✓	✓	5.51	9.24	16.65	22.10	7.11	6.23	11.14
	$N'=700$	✓		✓	✓	5.80	9.32	16.61	21.86	7.15	6.28	11.17
(c)	w/ Traditional	✓	✓		✓	4.43	8.89	16.19	21.64	5.44	5.14	10.29
	w/o Encoding	✓	✓		✓	4.66	8.80	16.32	21.77	5.60	5.37	10.42
(d)	w/o Weight	✓	✓	✓		5.04	8.98	16.48	21.80	6.14	5.85	10.71
	w/ Loss L_{con}	✓	✓	✓	✓	4.35	8.90	16.20	21.77	5.34	5.17	10.29
	w/ Loss L_{MSE}	✓	✓	✓	✓	10.96	12.68	19.76	24.76	13.26	11.29	15.45
(e)	Full $N=600$	✓	✓	✓	✓	4.25	**8.69**	16.20	21.78	5.11	4.92	10.16
	Full $N=800$	✓	✓	✓	✓	4.30	8.73	**16.19**	**21.53**	5.08	5.04	10.15
	Final $N=700$	✓	✓	✓	✓	**4.17**	8.78	16.25	21.61	**4.98**	**4.86**	**10.11**

condition code C without any encoding processing. The results show that our learnable encoding scheme can bring performance improvement, and also reduce the necessity of selecting specific encoding functions in the traditional one.

(d) Output Module. We use a weighted maxpooling operation in Eq. (9) to recover the query point normal $\mathbf{n}_p$ from the hyper surface fitting results. Here, we estimate the normal as $\mathbf{n}_p = \mathcal{H}(\mathrm{MAX}\{\mathcal{N}_{\theta,\tau}(G_i, C_i)|i = 1, ..., N\})$ without using the weight. Moreover, we also evaluate other two models: 1) trained with an additional weighted neighborhood consistency loss $L_{con} = \frac{1}{N}\sum_{i=1}^{N} w_i|\hat{\mathbf{n}}_i \times \mathbf{n}_i|$ where the neighboring point normals are predicted by another function $\mathbf{n}_i = \mathcal{H}'(\mathcal{N}_{\theta,\tau}(G_i, C_i))$; 2) trained with the MSE loss L_{MSE} instead of the sin loss. The results are shown in Table 2(d), we can observe that: 1) the weight indeed improves the results; 2) the further added consistency loss L_{con} is not helpful for the final results, which means that we only need the query point normal in each point cloud patch and omit the neighboring point normals (also reduce network parameters); 3) the loss L_{MSE} can not guide the model to learn accurate normals.

(e) Input Patch Size. In the previous experiments, we set the input point cloud patch size to 700. In Table 2(e), we evaluate two full models with different patch sizes $N=600$ and $N=800$. The larger size brings better results than the smaller size under large noise, but takes more time and memory.

5 Conclusion

In this paper, we solved several problems in existing point cloud normal estimation methods. We propose to directly regress point normal vectors through a novel hyper surface fitting technique, which implicitly learns hyper surfaces from noisy 3D points in a high dimensional feature space, rather than fitting a geometric plane or surface using a polynomial function of a predefined order. Furthermore, we propose two novel modules, i.e. Space Transformation and Relative Position Encoding, to transform the 3D point clouds into the feature space from different spatial dimensions. We show that these two new designs are more effective than their respective counterparts. The combination of these modules (formed as HSurf-Net) reduces the influence of noise and outliers on the fitting process and improves the robustness and accuracy of normal estimation. Extensive experiments prove the effectiveness of HSurf-Net, and demonstrate that it produces visually and quantitatively better results than the state-of-the-art methods. The future works include exploring more effective point cloud representations, e.g. 3D voxel grids, and more efficient local feature extraction for normal estimation.

References

[1] Marc Alexa, Johannes Behr, Daniel Cohen-Or, Shachar Fleishman, David Levin, and Claudio T Silva. Point set surfaces. In *Proceedings Visualization, 2001. VIS'01.*, pages 21–29. IEEE, 2001.

[2] Pierre Alliez, David Cohen-Steiner, Yiying Tong, and Mathieu Desbrun. Voronoi-based variational reconstruction of unoriented point sets. In *Symposium on Geometry processing*, volume 7, pages 39–48, 2007.

[3] Nina Amenta and Marshall Bern. Surface reconstruction by voronoi filtering. *Discrete & Computational Geometry*, 22(4):481–504, 1999.

[4] Samir Aroudj, Patrick Seemann, Fabian Langguth, Stefan Guthe, and Michael Goesele. Visibility-consistent thin surface reconstruction using multi-scale kernels. *ACM Trans. Graph.*, 36(6):187–1, 2017.

[5] Haim Avron, Andrei Sharf, Chen Greif, and Daniel Cohen-Or. L1-sparse reconstruction of sharp point set surfaces. *ACM Transactions on Graphics (TOG)*, 29(5):1–12, 2010.

[6] Yizhak Ben-Shabat and Stephen Gould. DeepFit: 3D surface fitting via neural network weighted least squares. In *European Conference on Computer Vision*, pages 20–34. Springer, 2020.

[7] Yizhak Ben-Shabat, Michael Lindenbaum, and Anath Fischer. Nesti-net: Normal estimation for unstructured 3D point clouds using convolutional neural networks. In *Proceedings of the IEEE Conference on Computer Vision and Pattern Recognition*, pages 10112–10120, 2019.

[8] James F Blinn. Simulation of wrinkled surfaces. *ACM SIGGRAPH computer graphics*, 12(3):286–292, 1978.

[9] Alexandre Boulch and Renaud Marlet. Fast and robust normal estimation for point clouds with sharp features. In *Computer graphics forum*, volume 31, pages 1765–1774. Wiley Online Library, 2012.

[10] Alexandre Boulch and Renaud Marlet. Deep learning for robust normal estimation in unstructured point clouds. In *Computer Graphics Forum*, volume 35, pages 281–290. Wiley Online Library, 2016.

[11] Junjie Cao, Hairui Zhu, Yunpeng Bai, Jun Zhou, Jinshan Pan, and Zhixun Su. Latent tangent space representation for normal estimation. *IEEE Transactions on Industrial Electronics*, 69(1):921–929, 2021.

[12] Frédéric Cazals and Marc Pouget. Estimating differential quantities using polynomial fitting of osculating jets. *Computer Aided Geometric Design*, 22(2):121–146, 2005.

[13] Tamal K Dey and Samrat Goswami. Provable surface reconstruction from noisy samples. *Computational Geometry*, 35(1-2):124–141, 2006.

[14] Henri Gouraud. Continuous shading of curved surfaces. *IEEE transactions on computers*, 100(6):623–629, 1971.

[15] Gaël Guennebaud and Markus Gross. Algebraic point set surfaces. In *ACM SIGGRAPH 2007 papers*, pages 23–es. 2007.

[16] Paul Guerrero, Yanir Kleiman, Maks Ovsjanikov, and Niloy J Mitra. PCPNet: learning local shape properties from raw point clouds. In *Computer Graphics Forum*, volume 37, pages 75–85. Wiley Online Library, 2018.

[17] Meng-Hao Guo, Jun-Xiong Cai, Zheng-Ning Liu, Tai-Jiang Mu, Ralph R Martin, and Shi-Min Hu. PCT: Point cloud transformer. *Computational Visual Media*, 7(2):187–199, 2021.

[18] Timo Hackel, N. Savinov, L. Ladicky, Jan D. Wegner, K. Schindler, and M. Pollefeys. SEMANTIC3D.NET: A new large-scale point cloud classification benchmark. In *ISPRS Annals of the Photogrammetry, Remote Sensing and Spatial Information Sciences*, volume IV-1-W1, pages 91–98, 2017.

[19] Taisuke Hashimoto and Masaki Saito. Normal estimation for accurate 3D mesh reconstruction with point cloud model incorporating spatial structure. In *CVPR Workshops*, pages 54–63, 2019.

[20] Hugues Hoppe, Tony DeRose, Tom Duchamp, John McDonald, and Werner Stuetzle. Surface reconstruction from unorganized points. In *Proceedings of the 19th annual conference on Computer graphics and interactive techniques*, pages 71–78, 1992.

[21] Binh-Son Hua, Quang-Hieu Pham, Duc Thanh Nguyen, Minh-Khoi Tran, Lap-Fai Yu, and Sai-Kit Yeung. Scenenn: A scene meshes dataset with annotations. In *2016 Fourth International Conference on 3D Vision (3DV)*, pages 92–101. IEEE, 2016.

[22] Hui Huang, Dan Li, Hao Zhang, Uri Ascher, and Daniel Cohen-Or. Consolidation of unorganized point clouds for surface reconstruction. *ACM transactions on graphics (TOG)*, 28(5):1–7, 2009.

[23] Hui Huang, Shihao Wu, Minglun Gong, Daniel Cohen-Or, Uri Ascher, and Hao Zhang. Edge-aware point set resampling. *ACM transactions on graphics (TOG)*, 32(1):1–12, 2013.

[24] Robert A Jacobs, Michael I Jordan, Steven J Nowlan, and Geoffrey E Hinton. Adaptive mixtures of local experts. *Neural computation*, 3(1):79–87, 1991.

[25] Michael Kazhdan, Matthew Bolitho, and Hugues Hoppe. Poisson surface reconstruction. In *Proceedings of the fourth Eurographics symposium on Geometry processing*, volume 7, 2006.

[26] Carsten Lange and Konrad Polthier. Anisotropic smoothing of point sets. *Computer Aided Geometric Design*, 22(7):680–692, 2005.

[27] Thibault Lejemble, David Coeurjolly, Loic Barthe, and Nicolas Mellado. Stable and efficient differential estimators on oriented point clouds. In *Computer Graphics Forum*, volume 40, pages 205–216. Wiley Online Library, 2021.

[28] Jan Eric Lenssen, Christian Osendorfer, and Jonathan Masci. Deep iterative surface normal estimation. In *Proceedings of the IEEE/CVF Conference on Computer Vision and Pattern Recognition*, pages 11247–11256, 2020.

[29] David Levin. The approximation power of moving least-squares. *Mathematics of computation*, 67(224):1517–1531, 1998.

[30] Dening Lu, Xuequan Lu, Yangxing Sun, and Jun Wang. Deep feature-preserving normal estimation for point cloud filtering. *Computer-Aided Design*, 125:102860, 2020.
[31] Xuequan Lu, Scott Schaefer, Jun Luo, Lizhuang Ma, and Ying He. Low rank matrix approximation for 3D geometry filtering. *IEEE Transactions on Visualization and Computer Graphics*, 2020.
[32] Xuequan Lu, Shihao Wu, Honghua Chen, Sai-Kit Yeung, Wenzhi Chen, and Matthias Zwicker. Gpf: Gmm-inspired feature-preserving point set filtering. *IEEE transactions on visualization and computer graphics*, 24(8):2315–2326, 2017.
[33] Quentin Mérigot, Maks Ovsjanikov, and Leonidas J Guibas. Voronoi-based curvature and feature estimation from point clouds. *IEEE Transactions on Visualization and Computer Graphics*, 17(6):743–756, 2010.
[34] Niloy J Mitra and An Nguyen. Estimating surface normals in noisy point cloud data. In *Proceedings of the nineteenth annual symposium on Computational geometry*, pages 322–328, 2003.
[35] Mark Pauly, Markus Gross, and Leif P Kobbelt. Efficient simplification of point-sampled surfaces. In *IEEE Visualization, 2002. VIS 2002.*, pages 163–170. IEEE, 2002.
[36] Bui Tuong Phong. Illumination for computer generated pictures. *Communications of the ACM*, 18(6):311–317, 1975.
[37] Charles R Qi, Hao Su, Kaichun Mo, and Leonidas J Guibas. PointNet: Deep learning on point sets for 3D classification and segmentation. In *Proceedings of the IEEE conference on computer vision and pattern recognition*, pages 652–660, 2017.
[38] Charles Ruizhongtai Qi, Li Yi, Hao Su, and Leonidas J Guibas. PointNet++: Deep hierarchical feature learning on point sets in a metric space. *Advances in neural information processing systems*, 30:5099–5108, 2017.
[39] Riccardo Roveri, A Cengiz Öztireli, Ioana Pandele, and Markus Gross. Pointpronets: Consolidation of point clouds with convolutional neural networks. In *Computer Graphics Forum*, volume 37, pages 87–99. Wiley Online Library, 2018.
[40] Michael D Spivak. *A comprehensive introduction to differential geometry*. Publish or perish, 1970.
[41] Gilbert W Stewart. On the early history of the singular value decomposition. *SIAM review*, 35(4):551–566, 1993.
[42] Yujing Sun, Scott Schaefer, and Wenping Wang. Denoising point sets via l0 minimization. *Computer Aided Geometric Design*, 35:2–15, 2015.
[43] Ashish Vaswani, Noam Shazeer, Niki Parmar, Jakob Uszkoreit, Llion Jones, Aidan N Gomez, Łukasz Kaiser, and Illia Polosukhin. Attention is all you need. *Advances in neural information processing systems*, 30, 2017.
[44] Jie Zhang, Jun-Jie Cao, Hai-Rui Zhu, Dong-Ming Yan, and Xiu-Ping Liu. Geometry guided deep surface normal estimation. *Computer-Aided Design*, 142:103119, 2022.
[45] Hengshuang Zhao, Li Jiang, Jiaya Jia, Philip HS Torr, and Vladlen Koltun. Point transformer. In *Proceedings of the IEEE/CVF International Conference on Computer Vision*, pages 16259–16268, 2021.
[46] Haoran Zhou, Honghua Chen, Yidan Feng, Qiong Wang, Jing Qin, Haoran Xie, Fu Lee Wang, Mingqiang Wei, and Jun Wang. Geometry and learning co-supported normal estimation for unstructured point cloud. In *Proceedings of the IEEE/CVF Conference on Computer Vision and Pattern Recognition*, pages 13238–13247, 2020.
[47] Haoran Zhou, Honghua Chen, Yingkui Zhang, Mingqiang Wei, Haoran Xie, Jun Wang, Tong Lu, Jing Qin, and Xiao-Ping Zhang. Refine-Net: Normal refinement neural network for noisy point clouds. *IEEE Transactions on Pattern Analysis and Machine Intelligence*, 2022.
[48] Jun Zhou, Hua Huang, Bin Liu, and Xiuping Liu. Normal estimation for 3D point clouds via local plane constraint and multi-scale selection. *Computer-Aided Design*, 129:102916, 2020.
[49] Jun Zhou, Wei Jin, Mingjie Wang, Xiuping Liu, Zhiyang Li, and Zhaobin Liu. Improvement of normal estimation for point clouds via simplifying surface fitting. *arXiv preprint arXiv:2104.10369*, 2021.
[50] Runsong Zhu, Yuan Liu, Zhen Dong, Yuan Wang, Tengping Jiang, Wenping Wang, and Bisheng Yang. AdaFit: Rethinking learning-based normal estimation on point clouds. In *Proceedings of the IEEE/CVF International Conference on Computer Vision*, pages 6118–6127, 2021.

Checklist

1. For all authors...
   (a) Do the main claims made in the abstract and introduction accurately reflect the paper's contributions and scope? [Yes]
   (b) Did you describe the limitations of your work? [Yes] In the supplemental materials.
   (c) Did you discuss any potential negative societal impacts of your work? [Yes] In the supplemental materials.
   (d) Have you read the ethics review guidelines and ensured that your paper conforms to them? [Yes]
2. If you are including theoretical results...

(a) Did you state the full set of assumptions of all theoretical results? [Yes]

(b) Did you include complete proofs of all theoretical results? [Yes]

3. If you ran experiments...

(a) Did you include the code, data, and instructions needed to reproduce the main experimental results (either in the supplemental material or as a URL)? [Yes]

(b) Did you specify all the training details (e.g., data splits, hyperparameters, how they were chosen)? [Yes]

(c) Did you report error bars (e.g., with respect to the random seed after running experiments multiple times)? [No] It would be too computationally expensive.

(d) Did you include the total amount of compute and the type of resources used (e.g., type of GPUs, internal cluster, or cloud provider)? [Yes]

4. If you are using existing assets (e.g., code, data, models) or curating/releasing new assets...

(a) If your work uses existing assets, did you cite the creators? [Yes]

(b) Did you mention the license of the assets? [No] We were unable to find the license for the dataset we used.

(c) Did you include any new assets either in the supplemental material or as a URL? [Yes]

(d) Did you discuss whether and how consent was obtained from people whose data you're using/curating? [No]

(e) Did you discuss whether the data you are using/curating contains personally identifiable information or offensive content? [No]

5. If you used crowdsourcing or conducted research with human subjects...

(a) Did you include the full text of instructions given to participants and screenshots, if applicable? [N/A]

(b) Did you describe any potential participant risks, with links to Institutional Review Board (IRB) approvals, if applicable? [N/A]

(c) Did you include the estimated hourly wage paid to participants and the total amount spent on participant compensation? [N/A]

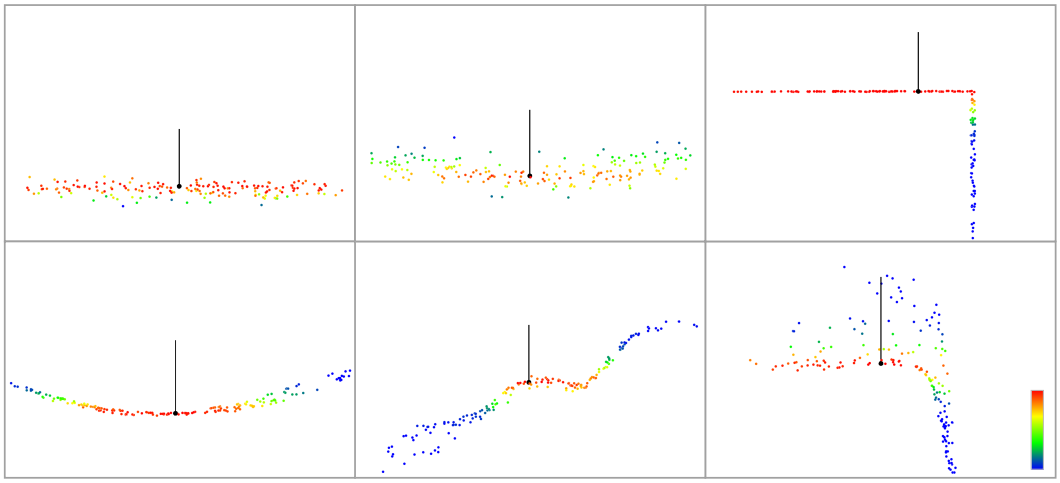

Figure 7: Visualization of the contribution of each 3D point to the normal estimate of the query point (black). The red points are weighted higher than the blue points.

A Appendix

A.1 Notations

n	The order of polynomial function
$\mathbf{n}$	The point normal vector
α, β	The coefficient of polynomial function
N_n	The number of terms in the coefficient
$P = \{p_i \vert i = 1, ..., N\}$	Input point cloud
$p = (x, y, z)$	A point and its coordinate
$f(x, y)$	The height function in 3D space
S	A smooth surface in 3D space
$O(\cdot)$	The remainder in Taylor's multivariate formula
J, J^*	The polynomial function and its optimal solution
$\mathcal{N}, \mathcal{N}^*$	The hyper surface and its optimal solution
τ	The order of hyper surface (i.e., parameters of an MLP)
θ	The coefficient of hyper surface (i.e., parameters of an MLP)
(G, C, F)	The high dimensional feature space
G	The global location code from Space Transformation module
C	The condition code from Relative Position Encoding module
$\mathcal{F}$	The height function in feature space
N, M	The number of points in the point cloud patch
N_s	The neighborhood size of the query point p at scale s
N_k	The per-point neighborhood size in the Relative Position Encoding
$\mathcal{H}, \Psi$	MLP Layers in the Hyper Surface Fitting
$\mathcal{U}, \mathcal{V}$	MLP Layers in the Global Shift Layer
$\mathcal{E}, \phi$	MLP Layers in the Relative Position Encoding
$\mathrm{MAX}\{\cdot\}$	Maxpooling operation

A.2 Point Weight Visualization

In our algorithm, we use the hyper surface fitting results to predict the query point normal using an output module, in which we quantify each point's contribution to the final result by computing a weight $w_i = \mathrm{sigmod}(\Psi(\mathcal{N}_{\theta,\tau}(G_i, C_i)))$. In Fig. 7, we show each point's contribution in a point cloud patch to the query point normal estimation. We can see that the red points and the query point are basically on the same plane.